LETTERS

High-performance genetically targetable optical neural silencing by light-driven proton pumps

Brian Y. Chow[1,2]*, Xue Han[1,2]*, Allison S. Dobry[1,2], Xiaofeng Qian[1,2], Amy S. Chuong[1,2], Mingjie Li[1,2], Michael A. Henninger[1,2], Gabriel M. Belfort[2], Yingxi Lin[2], Patrick E. Monahan[1,2] & Edward S. Boyden[1,2]

The ability to silence the activity of genetically specified neurons in a temporally precise fashion would provide the opportunity to investigate the causal role of specific cell classes in neural computations, behaviours and pathologies. Here we show that members of the class of light-driven outward proton pumps can mediate powerful, safe, multiple-colour silencing of neural activity. The gene archaerhodopsin-3 (Arch)[1] from *Halorubrum sodomense* enables near-100% silencing of neurons in the awake brain when virally expressed in the mouse cortex and illuminated with yellow light. Arch mediates currents of several hundred picoamps at low light powers, and supports neural silencing currents approaching 900 pA at light powers easily achievable *in vivo*. Furthermore, Arch spontaneously recovers from light-dependent inactivation, unlike light-driven chloride pumps that enter long-lasting inactive states in response to light. These properties of Arch are appropriate to mediate the optical silencing of significant brain volumes over behaviourally relevant timescales. Arch function in neurons is well tolerated because pH excursions created by Arch illumination are minimized by self-limiting mechanisms to levels comparable to those mediated by channelrhodopsins[2,3] or natural spike firing. To highlight how proton pump ecological and genomic diversity may support new innovation, we show that the blue–green light-drivable proton pump from the fungus *Leptosphaeria maculans*[4] (Mac) can, when expressed in neurons, enable neural silencing by blue light, thus enabling alongside other developed reagents the potential for independent silencing of two neural populations by blue versus red light. Light-driven proton pumps thus represent a high-performance and extremely versatile class of 'optogenetic' voltage and ion modulator, which will broadly enable new neuroscientific, biological, neurological and psychiatric investigations.

We screened type I microbial opsins (see Supplementary Table 1) from archaebacteria, bacteria, plants and fungi for light-driven hyperpolarizing capability[5]. Mammalian codon-optimized genes were synthesized, cloned into green fluorescent protein (GFP)-fusion expression vectors, and transfected into cultured neurons. We measured opsin photocurrents and cell capacitance-normalized photocurrent densities under stereotyped illumination conditions (Fig. 1a, black and grey bars, respectively), as well as opsin action spectra (photocurrent as a function of wavelength; Supplementary Table 2). From this information, we estimated the photocurrent density for each opsin at its own spectral peak (Fig. 1a, white bars). For comparison purposes, we included an earlier-characterized microbial opsin, the *Natronomonas pharaonis* halorhodopsin (Halo/NpHR)—a light-driven inward chloride pump capable of modest hyperpolarizing currents[6–9]. Archaerhodopsin-3 from *H. sodomense* (Arch/aR-3), proposed to be a proton pump[1], generated large photocurrents in the screen, as did two other proton pumps, the *Leptosphaeria maculans* opsin (Mac/LR/Ops)[4] and cruxrhodopsin-1 (ref. 10) (albeit less than that of Arch; Fig. 1a). All light-driven chloride pumps assessed had lower screen photocurrents than these light-driven proton pumps.

Arch is a yellow–green light-sensitive (Fig. 1b) opsin that seems to express well on the neural plasma membrane (Fig. 1c; see Supplementary Notes on Arch expression levels and enhancing Arch membrane trafficking). Arch-mediated currents exhibited excellent kinetics of light-activation and post-light recovery. After illumination, Arch currents rose with a 15–85% onset time of 8.8 ± 1.8 ms (mean $\pm$ standard error (s.e.) reported throughout, unless otherwise indicated; $n = 16$ neurons), and after light cessation, Arch currents fell with an 85–15% offset time of 19.3 ± 2.9 ms. Under continuous yellow illumination, Arch photocurrent declined (Fig. 1d, e), as did the photocurrents of all of the opsins in our screen. However, unlike all of the halorhodopsins we screened (including products of halorhodopsin site-directed mutagenesis aimed at improving kinetics; Supplementary Table 3), which after illumination remained inactivated for long periods of time (for example, tens of minutes, with accelerated recovery requiring more blue light[6,11]), Arch spontaneously recovered function in seconds (Fig. 1d, e), more like the light-gated cation channel channelrhodopsin-2 from *Chlamydomonas reinhardtii* (ChR2)[2,3]. The magnitude of Arch-mediated photocurrents was large. At low light irradiances of 0.35 and 1.28 mW mm^{-2} (Fig. 1f, left), neural Arch currents were 120 and 189 pA, respectively; at higher light powers (for example, at which Halo currents saturate), Arch currents continued to increase, approaching 900 pA at effective irradiances of 36 mW mm^{-2}, well within the reach of typical *in vivo* experiments (Fig. 1f, right; see Methods for how effective irradiances were calculated). The high dynamic range of Arch may enable the use of light sources (for example, light-emitting diodes (LEDs), lasers) that are safe and effective for optical control *in vivo*[12,13].

Several lines of evidence supported the idea that Arch functioned as an outward proton pump when expressed in neurons. Removing the endogenous ions that commonly subserve neural inhibition, Cl$^-$ and K$^+$, from physiological solutions did not alter photocurrent magnitude ($P > 0.4$ comparing either K$^+$-free or Cl$^-$-free solutions to regular solutions, t-test; Fig. 2a). In solutions lacking Na$^+$, K$^+$, Cl$^-$ and Ca^{2+}, photocurrents were still no different from those measured in normal solutions ($P > 0.4$; $n = 4$ neurons tested without these four charge carriers). The reversal potential appeared to be less than -120 mV (Fig. 2b), also consistent with Arch being a proton pump.

We assessed the voltage swings driven by illumination of current-clamped Arch-expressing cultured neurons. As effective irradiance increased from 7.8 mW mm^{-2} to 36.3 mW mm^{-2} (Fig. 1f), voltage-clamped neurons exhibited peak currents that increased from

---

[1]The MIT Media Laboratory, Synthetic Neurobiology Group, and Department of Biological Engineering, [2]Department of Brain and Cognitive Sciences and MIT McGovern Institute for Brain Research, Massachusetts Institute of Technology, Cambridge, Massachusetts 02139, USA.
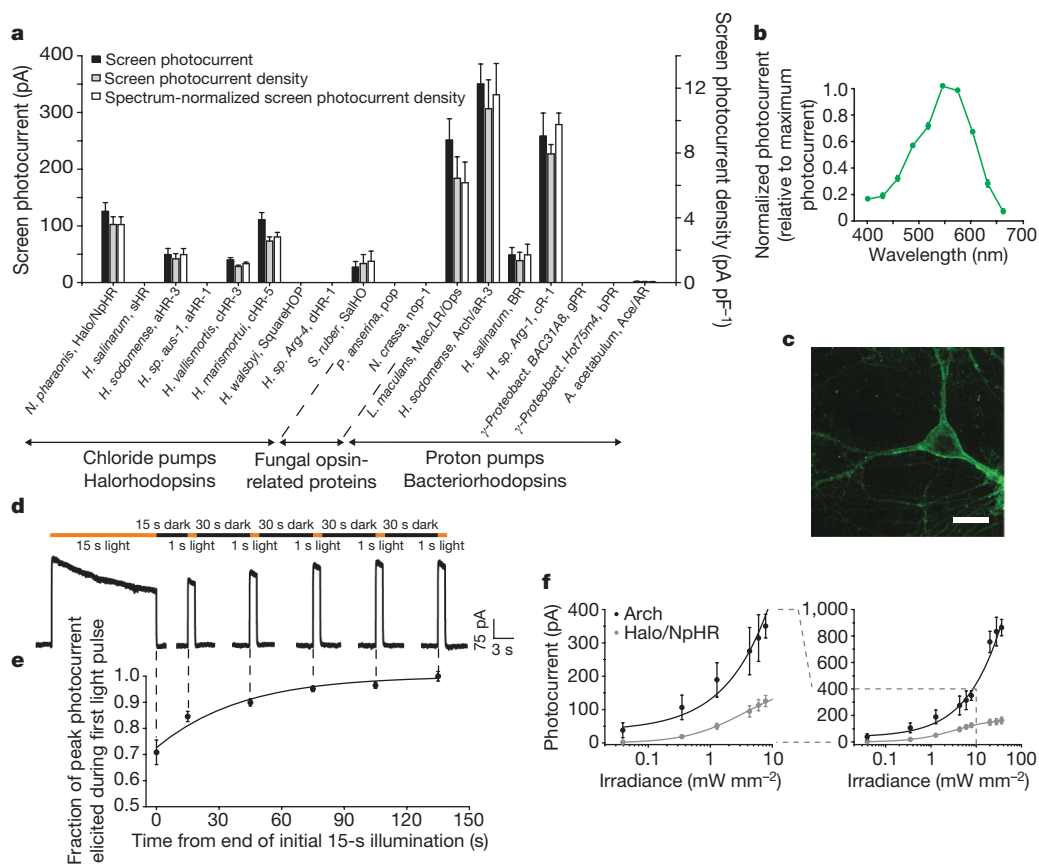*These authors contributed equally to this work.

Figure 1 | Optical neural silencing by light-driven proton pumping, revealed by a cross-kingdom functional molecular screen. a, Screen data showing outward photocurrents (left y axis, black bars), photocurrent densities (right y axis, grey bars), and action spectrum-normalized photocurrent densities (right y axis, white bars), measured by whole-cell patch-clamp of cultured neurons under screening illumination conditions (575 ± 25 nm, 7.8 mW mm^{-2} for all except Mac/LR/Ops, gPR, bPR and Ace/AR, which were 535 ± 25 nm, 9.4 mW mm^{-2}; see Supplementary Table 1 for details on the molecules screened; $n = 4$–16 neurons for each bar). Data are mean and s.e. Full species names from left to right: *Natronomonas pharaonis, Halobacterium salinarum, Halorubrum sodomense, Haloarcula vallismortis, Haloarcula marismortui, Haloquadratum walsbyi, Haloterrigena species Arg-4, Salinibacter ruber, Podospora anserina, Neurospora crassa, Leptosphaeria maculans, Halorubrum sodomense, Halobacterium salinarum, Haloarcula species Arg-1, uncultured gamma-proteobacterium BAC31A8,*

uncultured gamma-proteobacterium Hot75m4 and *Acetabularia acetabulum*[5]. **b,** Action spectrum of Arch measured in cultured neurons by scanning illumination light wavelength through the visible spectrum ($n = 7$ neurons). **c,** Confocal fluorescence image of a lentivirally infected cultured neuron expressing Arch–GFP. Scale bar, 20 μm. **d,** Raw current trace of a neuron lentivirally infected with Arch, illuminated by a 15-s light pulse (575 ± 25 nm, irradiance 7.8 mW mm^{-2}) followed by 1-s test pulses delivered at 15, 45, 75, 105 and 135 s after the end of the 15-s light pulse. **e,** Population data of averaged Arch photocurrents ($n = 11$ neurons) sampled at the times indicated by the vertical dotted lines that extend into **d. f,** Photocurrents of Arch versus Halo measured as a function of 575 ± 25 nm light irradiance (or effective light irradiance; see Methods for details), in patch-clamped cultured neurons ($n = 4$–16 neurons for each point), for low (left) and high (right) light powers. The line is a single Hill fit to the data.

350 ± 35 pA ($n = 16$ neurons) to 863 ± 62 pA ($n = 8$ neurons), respectively. Current-clamped neurons under these two irradiance conditions were hyperpolarized by −69.6 ± 7.3 mV ($n = 10$) and −76.2 ± 10.1 mV ($n = 8$), respectively. Notably, these voltage deflections, although both large, were not significantly different from one another ($P > 0.7$, t-test), suggesting the existence of a rapidly activated transporter or exchanger (perhaps the Na$^+$-dependent Cl$^-$/HCO$_3^-$ exchanger), or the opening of hyperpolarization-gated channels capable of shunting protons, which limit the effects of Arch on accumulated proton (or other charge carrier) gradients across neural membranes. This enabling of effective but not excessive silencing may make Arch safer than pumps that accumulate ions without self-regulation.

We next assessed the changes in intracellular pH (pH$_i$) driven by illumination of Arch-expressing cultured neurons, using the fluorescent pH indicator carboxy-SNARF-1. Within 1 s of illumination with strong green light (Fig. 2c), pH$_i$ rose from 7.309 ± 0.011 to 7.431 ± 0.020, plateauing rapidly. pH$_i$ increased slightly further after 15 s of illumination to 7.461 ± 0.024 (Fig. 1e). The fast stabilization of pH$_i$ may reflect the same self-limiting influence that limits proton-mediated voltage swings as described earlier, and may contribute to the safe operation of Arch in neurons by preventing large pH$_i$ swings.

The changes in pH$_i$ observed here are comparable in magnitude to those observed during illumination of ChR2-expressing cells[14] (owing to the proton currents carried by ChR2; refs 3, 15), and are also within the magnitudes of changes observed during normal neural activity[16–19]. Passive electrical properties of neurons were not affected by Arch expression (Fig. 2e–g; $P > 0.6$ for each measure, t-test), nor was cell death ($P > 0.6$, $\chi^2 = 0.26$; Fig. 2d).

We estimated the tissue volumes that could be silenced, using *in vitro* experiments and computational modelling. In cultured neurons expressing Arch or a trafficking-improved variant of Halo, eNpHR[8,9], we somatically injected brief current pulses at magnitudes chosen to mimic the current drives of neurons in the intact nervous system[20–23]. We exposed these neurons to periods of 575 nm yellow light (0.35, 1.28 or 6 mW mm^{-2}, simulating irradiance ~1.7, 1.2 or 0.6 mm away from the tip of a 200-μm fibre emitting 200 mW mm^{-2} irradiance, as modelled by Monte Carlo methods; see Supplementary Fig. 3), and measured the reduction in spike rate for each condition (Fig. 3a). In general, Arch-expressing neurons were significantly more inhibited than eNpHR-expressing cells. According to our model and the 350 pA data in Fig. 3a, the increase in brain tissue volume that would be 45–55% optically silenced would be ~10 times larger for Arch than for eNpHR.
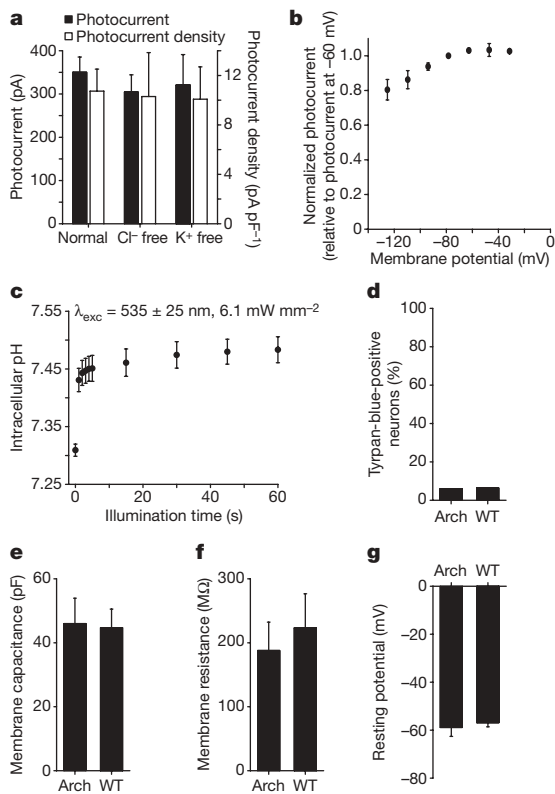
Figure 2 | Functional properties of the light-driven proton pump Arch in neurons. a, Photocurrent of Arch measured as a function of ionic composition (575 ± 25 nm light, 7.8 mW mm^{-2}), showing no significant dependence of photocurrent on the concentration of Cl$^-$ or K$^+$ ions in bath and intracellular solutions ($n = 16$, 8 and 7 neurons, from left to right). **b**, Arch proton photocurrent versus holding potential ($n = 4$ neurons). **c**, Intracellular pH measurements over a 1-min period of continuous illumination and simultaneous imaging (535 ± 25 nm light, 6.1 mW mm^{-2}) using SNARF-1 pH-sensitive ratiometric dye ($n = 10$–20 cells per data point). **d**, Trypan-blue staining of neurons lentivirally infected with Arch versus wild-type (WT) neurons, measured at 18 days *in vitro* ($n = 669$ Arch-expressing, 512 wild-type neurons). **e–g**, Membrane capacitance (**e**), membrane resistance (**f**), and resting potential (**g**) in neurons lentivirally infected with Arch versus wild-type neurons, measured at 11 days *in vitro* ($n = 7$ cells each).

To assess Arch *in vivo* directly, we injected lentivirus encoding for Arch into mouse cortex and recorded neural responses ~1 month later. Arch expressed well (Fig. 3b, left) and appeared well localized to the plasma membrane, labelling cell bodies, processes and dendritic spines (Fig. 3b, right). We recorded neurons in awake head-fixed mice, illuminating neurons by a 200-µm optical fibre coupled to a 593-nm laser (power at electrode tip estimated at ~3 mW mm^{-2}; refs 12, 13, 24). After light onset, firing rates of many units immediately and strongly declined, and remained low throughout the period of illumination, for both brief (Fig. 3c, top, d) and long (Fig. 3c, bottom) pulses. We recorded 13 single units that showed any decrease in firing during illumination, objectively identified as described in the Methods, and found spiking rates during exposure to 5 s yellow light (Fig. 3d) to drop by an average of $90 \pm 15\%$ (mean $\pm$ s.d.; Fig. 3e, f), restoring to levels indistinguishable from baseline after light cessation ($P > 0.2$, paired *t*-test; Fig. 3f). Six of the 13 units decreased spike rate by at least 99.5%, and the median decrease was 97.1% (Fig. 3g). One possibility is that Arch-expressing cells were almost completely silenced, whereas non-infected cells decreased activity owing to network activity reduction during illumination; note that only excitatory cells were genetically targeted here. Optical silencing was consistent across trials ($P > 0.1$, paired *t*-test comparing, for each neuron, responses to the first three versus the last three light exposures; ~20 trials per neuron). The kinetics of silencing were rapid: for the six neurons
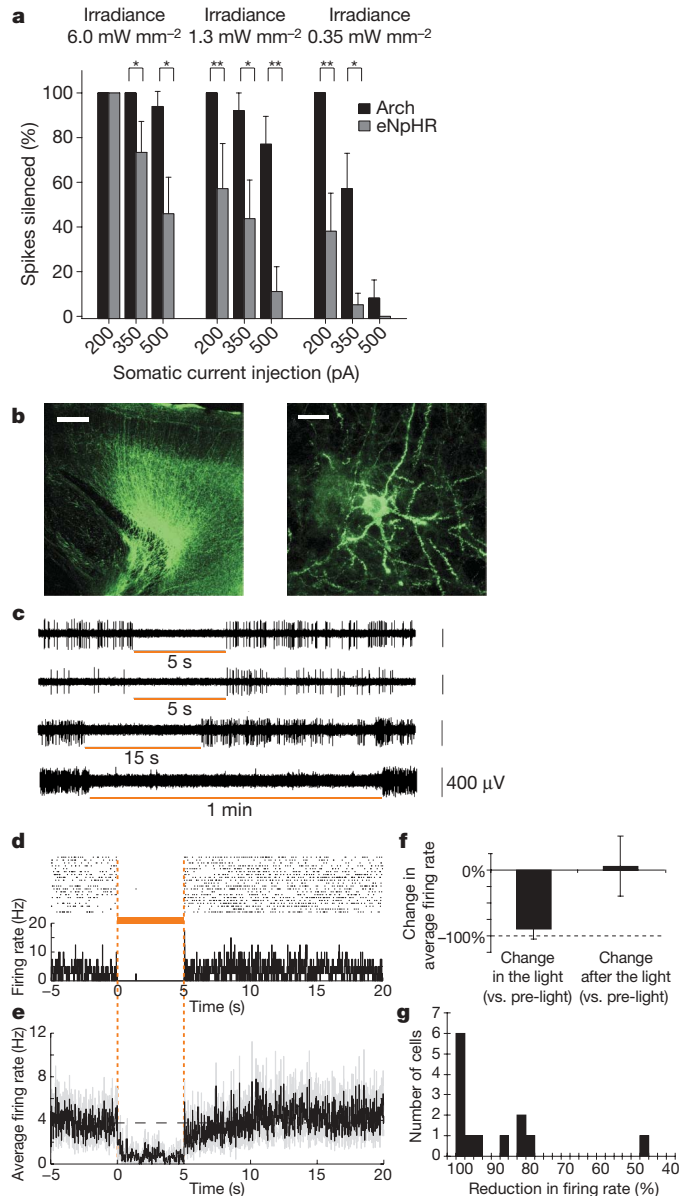

Figure 3 | High-performance Arch-mediated optical neural silencing of neocortical regions in awake mice. a, *In vitro* data showing, in cultured neurons expressing Arch or eNpHR and receiving trains of somatic current injections (15-ms pulse durations at 5 Hz), the per cent reduction of spiking under varying light powers (575 ± 25 nm light) as might be encountered *in vivo*. *$P < 0.05$, **$P < 0.01$, *t*-test. $n = 7$–8 cells for each condition. **b**, Fluorescence images showing Arch–GFP expression in mouse cortex ~1 month after lentiviral (FCK–Arch–GFP) injection. Scale bars, 200 µm (left) and 20 µm (right). **c**, Representative extracellular recordings showing neurons undergoing 5-s, 15-s and 1-min periods of light illumination (593 nm; ~150 mW mm^{-2} radiant flux out the fibre tip; and expected to be ~3 mW mm^{-2} at the electrode tip ~800 µm away^{12,13,24}). **d**, Neural activity in a representative neuron before, during and after 5 s of yellow light illumination, shown as a spike raster plot (top), and as a histogram of instantaneous firing rate averaged across trials (bottom; bin size, 20 ms). **e**, Population average of instantaneous firing rate before, during and after yellow light illumination (black line, mean; grey lines, mean $\pm$ s.e.; $n = 13$ units). **f**, Average change in spike firing during 5-s of yellow light illumination (left) and during the 5 s immediately after light offset (right), for the data shown in **d**. **g**, Histogram of percentage reductions in spike rate, for each individual neuron, integrated across all 5-s silencing period.

that underwent >99.5% silencing, spike firing reduced with near-0-ms latency, rarely firing spikes after light onset; averaged across all cells, firing-rate reductions plateaued within 229 ± 310 ms (mean $\pm$ s.d.) after light onset. After light cessation, firing rate restored quickly for

the highly silenced neurons; averaged across all cells, firing rates took 355 ± 505 ms to recover after light offset. The level of post-light firing did not vary with repeated light exposure ($P > 0.7$, paired t-test comparing, for each neuron, after-light firing rates during the first three versus the last three trials). Thus, Arch could mediate reliable, near-digital silencing of neurons in the awake mammalian brain.

Proton pumps naturally exist that are activated by many colours of light (see Supplementary Table 1), in contrast to chloride pumps, which are primarily driven by yellow–orange light (even with significant mutagenesis of retinal-flanking residues; Supplementary Table 3). The light-driven proton pump Mac (Fig. 1a), in our screen, had an action spectrum strongly blueshifted relative to that of the light-driven chloride pump Halo (Fig. 4a). We found that Mac-expressing neurons could undergo 4.1-fold larger hyperpolarizations with blue light than with red light, and Halo-expressing neurons could undergo 3.3-fold larger hyperpolarizations with red light than with blue light, when illuminated with appropriate filters (Fig. 4b). Accordingly, we could demonstrate selective silencing of spike firing in Mac-expressing neurons in response to blue light, and selective silencing of spike firing in Halo-expressing neurons in response to red light (Fig. 4c). Thus, the spectral diversity of proton pumps points the way towards independent multicolour silencing of separate neural populations. This
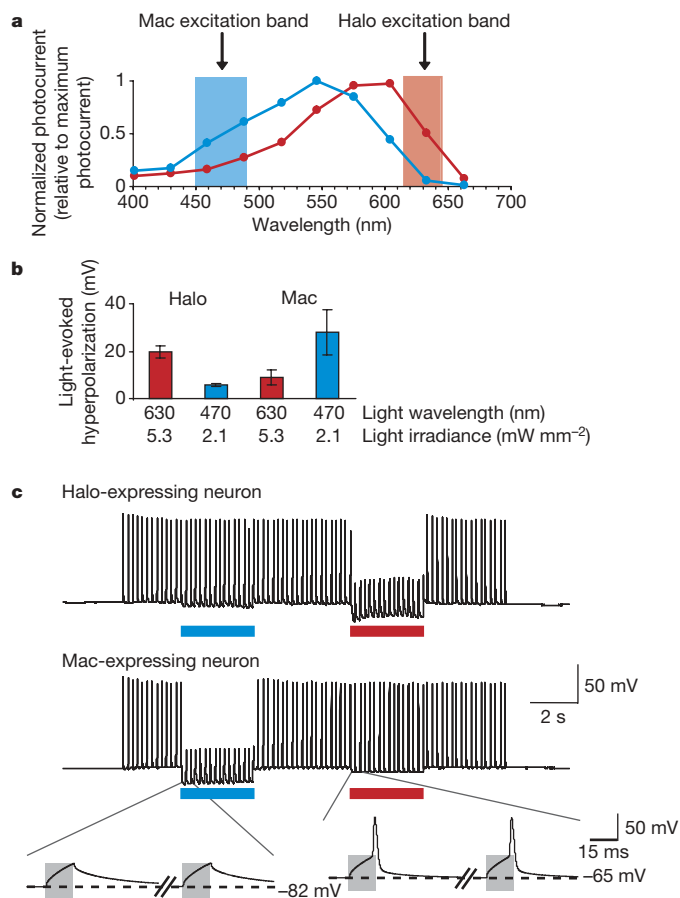
result opens up new kinds of experiment, in which, for example, two neuron classes, or two sets of neural projections from a single site, can be independently silenced during a behavioural task.

Arch and Mac represent members of a new, diverse and powerful class of optical neural silencing reagent, the light-driven proton pump, which operates without the need for exogenous chemical supplementation in mammalian cells. The efficacy of these proton pumps is surprising, given that protons occur, in mammalian tissue, at a million-fold lower concentration than the ions carried by other optical control molecules. This high efficacy may be due to the fast photocycle of Arch (see also refs 25, 26), but it may also be due to the ability of high-pK_a residues in proton pumps to mediate proton uptake[25,27]. We discovered several facts about this class of molecules that point the way for future neuroengineering innovation. First, proton pumping is a self-limiting process in neurons, providing for a safe and naturalistic form of neural silencing. Second, proton pumps recover spontaneously after optical activation, improving their relevance for behaviourally relevant silencing over the class of halorhodopsins. Finally, proton pumps exist with a wide diversity of action spectra, thus enabling multiple-colour silencing of distinct neural populations. Structure-guided mutagenesis of Arch and Mac may further facilitate development of neural silencers with altered spectrum or ion selectivity, given the significant amount of structure–function knowledge of the proton pump family (for example, refs 28–30).

Our study highlights the importance of ecological and genomic diversity in providing new molecular reagents for optical control of biological processes, as has previously benefited the fluorescent protein community. These opsins are likely to find uses across the spectrum of neuroscientific, biological and bioengineering fields. For example, expression of these opsins in neurons, muscle, immune cells and other excitable cells will allow control over their membrane potential, providing the opportunity to investigate the causal role of specific cells' activities in intact organisms, and, potentially, to understand the causal contribution of such cells to disease states in animal models. With the recent demonstration of the safe and efficacious use of the microbial opsin ChR2 to control neurons in non-human primates[24], it is in principle possible that in the future, these opsins may subserve new forms of neuromodulation technology that bear clinical benefit.

METHODS SUMMARY

Constructs with Arch, Mac and Halo are available at http://syntheticneurobiology.org/protocols. In brief, codon-optimized genes were synthesized by Genscript and fused to GFP in lentiviral and mammalian expression vectors as used previously[6,24] for transfection or viral infection of neurons. Primary hippocampal or cortical neurons were cultured and then transfected with plasmids or infected with viruses encoding for genes of interest, as described previously[6]. Images were taken using a Zeiss LSM 510 confocal microscope. Patch-clamp recordings were made using glass microelectrodes and a Multiclamp 700B/Digidata electrophysiology setup, using appropriate pipette and bath solutions for the experimental goal at hand. Neural pH imaging was done using carboxy-SNARF-1-AM ester (Invitrogen). Cell health was assayed using trypan blue staining (Gibco). HEK cells were cultured and patch-clamped using standard protocols. Mutagenesis was performed using the QuikChange kit (Stratagene). Computational modelling of light propagation was done with Monte Carlo simulation with MATLAB. *In vivo* recordings were made on head-fixed awake mice, which were surgically injected with lentivirus, and implanted with a headplate as described before[24]. Glass pipettes attached to laser-coupled optical fibres were inserted into the brain, to record neural activity during laser illumination in a photoelectrochemical artefact-free way. Data analysis was performed using Clampfit, Excel, Origin and MATLAB. Histology was performed using transcardial formalin perfusion followed by sectioning and subsequent confocal imaging.

Figure 4 | Multicolour silencing of two neural populations, enabled by blue- and red-light drivable ion pumps of different classes. a, Action spectra of Mac versus Halo; rectangles indicate filter bandwidths used for multicolour silencing *in vitro*. Blue light is delivered by a 470 ± 20 nm filter at 5.3 mW mm^{-2}, and red light is delivered by a 630 ± 15 nm filter at 2.1 mW mm^{-2}. **b**, Membrane hyperpolarizations elicited by blue versus red light, in cells expressing Halo or Mac ($n = 5$ Mac-expressing and $n = 6$ Halo-expressing neurons). **c**, Action potentials evoked by current injection into patch-clamped cultured neurons transfected with Halo (top) were selectively silenced by the red light but not by the blue light, and vice-versa in neurons expressing Mac (middle). Grey boxes in the inset (bottom) indicate periods of patch-clamp current injection.

1. Ihara, K. *et al.* Evolution of the archaeal rhodopsins: evolution rate changes by gene duplication and functional differentiation. *J. Mol. Biol.* **285**, 163–174 (1999).
2. Boyden, E. S., Zhang, F., Bamberg, E., Nagel, G. & Deisseroth, K. Millisecond-timescale, genetically targeted optical control of neural activity. *Nature Neurosci.* **8**, 1263–1268 (2005).

3. Nagel, G. et al. Channelrhodopsin-2, a directly light-gated cation-selective membrane channel. *Proc. Natl Acad. Sci. USA* **100**, 13940–13945 (2003).
4. Waschuk, S. A., Bezerra, A. G., Shi, L. & Brown, L. S. Leptosphaeria rhodopsin: Bacteriorhodopsin-like proton pump from a eukaryote. *Proc. Natl Acad. Sci. USA* **102**, 6879–6883 (2005).
5. Klare, J. P., Chizhov, I. & Engelhard, M. Microbial rhodopsins: scaffolds for ion pumps, channels, and sensors. *Results Probl. Cell Differ.* **45**, 73–122 (2008).
6. Han, X. & Boyden, E. S. Multiple-color optical activation, silencing, and desynchronization of neural activity, with single-spike temporal resolution. *PLoS One* **2**, e299 (2007).
7. Zhang, F. et al. Multimodal fast optical interrogation of neural circuitry. *Nature* **446**, 633–639 (2007).
8. Zhao, S. et al. Improved expression of halorhodopsin for light-induced silencing of neuronal activity. *Brain Cell Biol.* **36**, 141–154 (2008).
9. Gradinaru, V., Thompson, K. R. & Deisseroth, K. eNpHR: a Natronomonas halorhodopsin enhanced for optogenetic applications. *Brain Cell Biol.* **36**, 129–139 (2008).
10. Tateno, M., Ihara, K. & Mukohata, Y. The novel ion pump rhodopsins from *Haloarcula* form a family independent from both the bacteriorhodopsin and archaerhodopsin families/tribes. *Arch. Biochem. Biophys.* **315**, 127–132 (1994).
11. Bamberg, E., Tittor, J. & Oesterhelt, D. Light-driven proton or chloride pumping by halorhodopsin. *Proc. Natl Acad. Sci. USA* **90**, 639–643 (1993).
12. Aravanis, A. M. et al. An optical neural interface: in vivo control of rodent motor cortex with integrated fiberoptic and optogenetic technology. *J. Neural Eng.* **4**, S143–S156 (2007).
13. Bernstein, J. G. et al. Prosthetic systems for therapeutic optical activation and silencing of genetically-targeted neurons. *Proc. Soc. Photo Opt. Instrum. Eng.* **6854**, 68540H (2008).
14. Lin, J. Y., Lin, M. Z., Steinbach, P. & Tsien, R. Y. Characterization of engineered channelrhodopsin variants with improved properties and kinetics. *Biophys. J.* **96**, 1803–1814 (2009).
15. Berthold, P. et al. Channelrhodopsin-1 initiates phototaxis and photophobic responses in *Chlamydomonas* by immediate light-induced depolarization. *Plant Cell* **20**, 1665–1677 (2008).
16. Bevensee, M. O., Cummins, T. R., Haddad, G. G., Boron, W. F. & Boyarsky, G. pH regulation in single CA1 neurons acutely isolated from the hippocampi of immature and mature rats. *J. Physiol. (Lond.)* **494**, 315–328 (1996).
17. Chesler, M. Regulation and modulation of pH in the brain. *Physiol. Rev.* **83**, 1183–1221 (2003).
18. Meyer, T. M., Munsch, T. & Pape, H. C. Activity-related changes in intracellular pH in rat thalamic relay neurons. *Neuroreport* **11**, 33–36 (2000).
19. Trapp, S., Luckermann, M., Brooks, P. A. & Ballanyi, K. Acidosis of rat dorsal vagal neurons in situ during spontaneous and evoked activity. *J. Physiol. (Lond.)* **496**, 695–710 (1996).
20. Leinekugel, X. et al. Correlated bursts of activity in the neonatal hippocampus in vivo. *Science* **296**, 2049–2052 (2002).
21. Wehr, M. & Zador, A. M. Balanced inhibition underlies tuning and sharpens spike timing in auditory cortex. *Nature* **426**, 442–446 (2003).
22. Richter, D. W., Pierrefiche, O., Lalley, P. M. & Polder, H. R. Voltage-clamp analysis of neurons within deep layers of the brain. *J. Neurosci. Methods* **67**, 121–131 (1996).
23. Narikawa, K., Furue, H., Kumamoto, E. & Yoshimura, M. In vivo patch-clamp analysis of IPSCs evoked in rat substantia gelatinosa neurons by cutaneous mechanical stimulation. *J. Neurophysiol.* **84**, 2171–2174 (2000).
24. Han, X. et al. Millisecond-timescale optical control of neural dynamics in the nonhuman primate brain. *Neuron* **62**, 191–198 (2009).
25. Ming, M. et al. pH dependence of light-driven proton pumping by an archaerhodopsin from Tibet: comparison with bacteriorhodopsin. *Biophys. J.* **90**, 3322–3332 (2006).
26. Lukashev, E. P. et al. pH dependence of the absorption spectra and photochemical transformations of the archaerhodopsins. *Photochem. Photobiol.* **60**, 69–75 (1994).
27. Lanyi, J. K. Proton transfers in the bacteriorhodopsin photocycle. *Biochim. Biophys. Acta* **1757**, 1012–1018 (2006).
28. Enami, N. et al. Crystal structures of archaerhodopsin-1 and -2: common structural motif in archaeal light-driven proton pumps. *J. Mol. Biol.* **358**, 675–685 (2006).
29. Mogi, T., Marti, T. & Khorana, H. G. Structure-function studies on bacteriorhodopsin. IX. Substitutions of tryptophan residues affect protein-retinal interactions in bacteriorhodopsin. *J. Biol. Chem.* **264**, 14197–14201 (1989).
30. Luecke, H., Schobert, B., Richter, H. T., Cartailler, J. P. & Lanyi, J. K. Structure of bacteriorhodopsin at 1.55 Å resolution. *J. Mol. Biol.* **291**, 899–911 (1999).

Author Information Sequences are available to download from GenBank (http://www.ncbi.nlm.nih.gov/) under accession numbers: GU045593 (mammalian codon-optimized Arch), GU045594 (mammalian codon-optimized Arch fused to GFP), GU045595 (mammalian codon-optimized Mac), GU045596 (mammalian codon-optimized Mac fused to GFP), GU045597 (ss-Prl-Arch), GU045598 (ss-Arch-GFP-ER2) and GU045599 (ss-Prl-Arch-GFP). Reprints and permissions information is available at www.nature.com/reprints. The authors declare no competing financial interests. Correspondence and requests for materials should be addressed to E.S.B. (esb@media.mit.edu).